Electronic supplement: Realtime Selection of Optimal Source Parameters Using Ground Motion Envelopes

Dario Jozinović * [1], **John Clinton** [1], **Frédérick Massin** [1], **Maren Böse** [1], **Carlo Cauzzi** [1]

[1]Swiss Seismological Service, ETH Zurich, Zurich, Switzerland

Abstract Section 1 of the supplement contains the figures of average goodness-of-fit for different magnitude-distance perturbation pairs averaged taken over all 10 events in Table 1 (in the Manuscript) using different input time windows, and plots of some specific observed and predicted envelopes. Section 2 explains the generation of predicted envelopes and their adaptation to Switzerland.

1 Additional Figures

2 s window

Distance error (km)

Magnitude error	0	1	3	5	10	15	20	25	30	100	150
-1.50	21.94	20.18	18.19	15.72	14.06	8.09	4.24	3.82	2.12	0.00	0.00
-1.0	34.45	31.97	29.72	23.24	17.05	10.69	8.85	5.50	1.93	0.00	0.00
-0.9	37.77	35.17	30.10	27.48	19.37	8.11	4.94	3.11	3.72	0.00	0.00
-0.8	41.43	38.68	33.98	26.60	22.22	13.59	11.34	2.70	3.65	0.00	0.00
-0.7	45.36	42.48	33.27	29.13	23.81	17.01	7.12	8.04	3.27	0.36	0.00
-0.6	49.46	46.60	41.21	31.55	27.57	15.71	7.43	4.00	3.66	0.00	0.04
-0.5	53.26	50.93	44.55	34.35	25.98	18.77	12.77	4.01	3.99	0.05	0.00
-0.4	*56.89	*55.11	46.46	42.50	26.08	10.31	15.56	3.63	4.42	0.00	0.00
-0.3	*60.27	*58.63	50.03	40.56	30.81	16.98	8.31	4.15	4.55	0.05	0.00
-0.2	*63.07	*61.42	54.44	42.19	31.16	20.86	14.41	2.78	3.64	0.00	0.00
-0.1	*64.97	*64.13	*56.49	44.49	31.67	21.38	14.86	8.85	4.56	0.16	0.00
0.0	*66.10	*66.49	*59.11	50.27	33.93	14.42	8.44	3.57	2.64	0.00	0.00
0.1	*65.51	*67.39	*60.65	45.78	31.78	13.34	6.81	2.49	4.27	0.00	0.00
0.2	*64.54	*67.39	*62.35	44.73	26.27	21.94	12.07	1.25	2.86	0.00	0.00
0.3	*63.66	*67.33	*59.90	44.77	29.79	23.68	12.07	3.02	1.73	0.11	0.00
0.4	*62.42	*66.45	*59.09	43.19	30.64	24.24	6.02	7.65	2.61	0.00	0.00
0.5	*60.92	*64.91	*56.09	44.69	28.43	23.84	6.32	1.77	2.58	0.00	0.00
0.6	*58.88	*62.68	*55.73	39.22	28.16	13.08	6.55	9.56	3.34	0.08	0.00
0.7	*56.21	*59.56	52.76	35.05	31.77	21.71	5.69	2.55	1.34	0.02	0.06
0.8	53.22	*56.47	47.89	37.34	26.78	21.94	10.12	7.36	3.48	0.00	0.00
0.9	49.37	52.65	45.58	29.90	26.40	15.68	4.95	4.17	1.82	0.08	0.00
1.0	45.78	48.94	42.59	31.47	23.87	19.26	9.49	8.41	1.47	0.12	0.00
1.30	36.82	39.51	33.42	20.91	23.56	17.43	6.13	0.36	1.43	0.00	0.00

Figure S1 Average goodness-of-fit for different magnitude-epicentral distance perturbation pairs taken over all 10 events in Table 1 (in the Manuscript) using an input time window ending 2 seconds after the P-arrival at the closest station. The columns and rows show the errors in the source location (km) and magnitude, respectively. The small star in front of a number is used to mark the goodness-of-fit value higher than 55.

*Corresponding author: dario.jozinovic@sed.ethz.ch

3 s window

Distance error (km)

Magnitude error

	0	1	3	5	10	15	20	25	30	100	150
-1.50	19.02	19.69	18.32	18.93	12.49	9.67	6.76	4.78	2.99	0.60	0.00
-1.0	29.97	31.01	26.72	29.97	19.77	13.05	10.25	7.56	4.53	0.12	0.19
-0.9	32.56	33.67	32.30	32.97	22.74	15.28	11.51	7.79	4.80	0.21	0.00
-0.8	35.44	36.50	36.58	31.18	23.78	17.09	12.14	8.69	5.10	0.44	0.00
-0.7	38.55	39.35	38.11	33.75	25.62	19.14	13.08	8.66	5.36	0.00	0.05
-0.6	41.66	42.19	41.87	36.02	28.02	21.60	16.29	8.87	5.64	0.17	0.06
-0.5	44.61	44.76	42.20	42.96	31.00	21.56	14.70	9.28	5.77	0.00	0.00
-0.4	47.48	47.34	47.17	44.09	32.59	23.51	14.26	9.79	5.49	0.15	0.00
-0.3	49.96	49.61	47.88	46.57	35.30	23.02	14.19	10.59	6.48	0.00	0.00
-0.2	52.31	51.73	50.59	50.33	34.80	23.35	16.73	10.79	7.04	0.01	0.00
-0.1	54.66	53.95	53.98	51.64	36.78	23.56	18.84	9.55	6.04	0.51	0.05
0.0	⋆56.22	⋆55.69	53.61	51.18	39.13	26.68	17.64	11.32	4.04	0.01	0.00
0.1	⋆57.64	⋆56.86	⋆55.36	52.15	35.70	25.02	13.94	10.57	8.07	0.77	0.25
0.2	⋆57.80	⋆56.95	⋆57.36	52.14	32.87	17.47	17.72	9.72	4.08	0.06	0.16
0.3	⋆57.58	⋆56.82	⋆56.08	46.83	35.72	26.41	17.38	6.37	5.94	0.04	0.43
0.4	⋆56.24	⋆55.77	54.65	43.98	36.42	25.04	18.30	8.32	3.73	0.00	0.03
0.5	53.61	53.72	53.10	43.60	35.73	24.80	16.38	11.22	3.28	0.18	0.00
0.6	50.57	50.93	53.21	48.57	34.43	25.85	19.41	11.77	6.75	0.47	0.15
0.7	47.48	48.04	51.11	50.12	34.74	26.36	17.87	12.19	2.77	0.00	0.01
0.8	43.39	44.04	48.90	46.31	28.66	16.43	17.42	12.07	6.73	0.16	0.03
0.9	40.41	41.14	42.91	35.41	32.08	25.04	18.57	10.18	7.36	0.19	0.00
1.0	37.48	38.28	41.62	40.01	32.75	17.85	16.28	13.15	5.76	0.00	0.00
1.30	29.90	30.97	33.62	36.47	21.71	18.35	13.51	10.94	7.21	0.14	0.00

Figure S2 Same as Figure S1 for an input window ending 3 seconds after the first P-arrival at the closest station.

7 s window

Distance error (km)

Magnitude error

	0	1	3	5	10	15	20	25	30	100	150
-1.50	17.05	17.16	17.13	17.59	15.57	13.84	11.62	10.79	6.25	0.52	0.14
-1.0	28.16	28.36	28.55	28.61	27.42	22.21	16.69	13.52	8.51	0.14	0.17
-0.9	31.17	31.40	31.05	31.60	27.67	23.49	18.89	14.83	15.44	0.17	0.31
-0.8	34.52	34.69	35.00	34.18	32.00	24.77	19.77	15.50	9.69	0.65	0.16
-0.7	38.11	38.35	38.45	37.31	35.23	26.70	19.56	17.60	11.08	0.16	0.15
-0.6	42.02	42.71	41.85	41.42	37.59	29.95	22.53	19.05	12.52	0.45	0.25
-0.5	46.68	46.74	45.76	46.58	42.16	30.02	24.75	17.43	11.28	0.64	0.38
-0.4	50.74	50.84	51.42	48.35	43.24	31.43	24.09	17.43	12.36	0.35	0.15
-0.3	⋆55.22	⋆55.28	53.58	51.51	46.17	34.31	25.01	17.94	17.80	0.66	0.41
-0.2	⋆59.08	⋆59.25	⋆56.75	53.83	44.46	34.84	26.26	20.26	18.15	0.51	0.14
-0.1	⋆60.80	⋆60.86	⋆59.65	⋆55.88	44.80	35.46	27.19	22.15	15.22	0.60	0.14
0.0	⋆61.98	⋆61.97	⋆58.46	⋆55.88	47.15	35.53	26.94	21.11	14.80	0.67	0.18
0.1	⋆63.60	⋆62.95	⋆59.45	⋆56.83	47.17	35.27	28.22	20.12	13.90	0.57	0.15
0.2	⋆63.11	⋆62.87	⋆59.47	⋆57.64	48.47	37.81	27.52	21.88	17.61	0.70	0.17
0.3	⋆61.98	⋆62.03	⋆59.41	⋆57.02	45.72	36.14	29.04	23.20	18.07	0.42	0.28
0.4	⋆60.21	⋆60.00	⋆57.93	⋆55.07	45.13	33.34	27.61	23.49	14.45	0.57	0.16
0.5	⋆57.54	⋆57.46	54.59	52.70	43.98	34.43	28.91	21.93	16.47	0.51	0.26
0.6	54.60	54.61	53.89	49.83	41.76	32.57	27.09	19.37	17.09	1.30	0.24
0.7	51.28	50.96	48.31	47.18	39.62	31.50	27.45	20.29	17.04	0.45	0.16
0.8	47.52	47.42	45.14	44.11	38.44	30.43	23.24	23.54	16.63	0.65	0.18
0.9	44.89	43.76	42.38	41.80	34.24	28.54	21.33	15.53	19.87	0.73	0.32
1.0	41.68	40.95	39.04	38.25	33.26	28.03	21.11	23.17	19.49	0.72	0.20
1.30	33.44	32.96	31.85	31.35	28.84	23.96	19.06	20.09	8.78	0.35	0.15

Figure S3 Same as Figure S1 for an input window ending 7 seconds after the first P-arrival at the closest station.

40 s window

Distance error (km)

Magnitude error	0	1	3	5	10	15	20	25	30	100	150
-1.50	17.93	17.98	17.76	17.46	15.88	13.38	12.21	9.90	9.34	3.90	2.01
-1.0	30.33	30.23	29.81	29.06	27.03	23.37	19.96	18.75	15.73	7.55	4.27
-0.9	33.88	33.78	33.38	32.82	30.15	27.21	23.29	19.28	18.45	10.11	5.78
-0.8	37.68	37.56	37.19	36.41	33.74	29.38	25.18	21.85	20.91	10.06	5.95
-0.7	41.88	41.75	41.24	40.35	37.13	33.99	29.22	25.99	23.27	11.33	6.82
-0.6	46.57	46.43	45.98	44.78	42.19	37.24	32.40	28.94	25.47	12.54	8.41
-0.5	51.59	51.46	50.76	49.74	46.16	41.57	35.27	30.43	29.08	14.69	6.19
-0.4	*56.80	*56.66	*55.82	54.92	51.74	46.25	40.77	33.69	29.77	16.27	9.54
-0.3	*61.93	*61.80	*61.13	*59.85	*55.21	48.73	42.18	37.84	32.96	16.79	11.33
-0.2	*66.47	*66.35	*65.38	*64.04	*60.24	53.24	48.11	42.91	38.88	20.50	11.78
-0.1	*69.79	*69.71	*68.46	*67.18	*62.63	54.07	49.62	45.85	38.05	21.59	11.56
0.0	*71.32	*71.34	*71.15	*68.92	*63.06	*57.69	52.75	46.51	42.10	23.62	15.39
0.1	*70.93	*70.93	*69.78	*70.00	*62.75	*56.28	50.41	45.79	40.04	24.70	17.86
0.2	*68.99	*68.95	*67.55	*67.22	*61.03	54.84	48.43	46.55	43.81	26.46	19.74
0.3	*65.60	*65.63	*65.16	*62.66	*59.35	*55.79	45.51	46.78	37.59	25.83	20.08
0.4	*61.13	*61.16	*59.72	*58.92	54.38	52.23	45.64	44.39	40.47	25.98	20.95
0.5	*56.34	*56.49	*55.90	54.49	54.49	49.09	45.62	39.68	38.74	27.46	20.63
0.6	51.61	51.79	51.50	51.56	49.02	43.52	42.24	34.40	36.04	26.45	20.81
0.7	47.15	47.32	46.89	46.81	45.60	38.46	38.68	35.87	31.18	24.86	19.40
0.8	42.84	43.00	42.29	42.76	40.73	35.33	35.50	32.12	31.02	26.26	21.07
0.9	38.95	39.08	38.57	39.47	36.13	32.81	31.28	30.31	27.79	24.70	20.35
1.0	35.45	35.58	35.22	34.99	32.95	31.34	29.84	27.68	25.00	24.68	20.88
1.30	27.02	27.12	26.79	27.07	25.66	24.38	22.62	20.87	18.78	23.41	21.02

Figure S4 Same as Figure S1 for an input window ending 40 seconds after the first P-arrival at the closest station.

20 s window

Distance error (km)

Magnitude error	0	1	3	5	10	15	20	25	30	100	150
-1.50	17.96	17.95	17.76	17.35	14.34	11.09	7.75	6.73	5.83	1.69	0.22
-1.0	29.57	29.57	29.36	28.71	25.15	19.81	15.04	10.58	10.70	3.24	0.33
-0.9	32.81	32.80	32.37	31.73	27.51	21.76	16.37	13.42	11.63	3.68	0.36
-0.8	36.42	36.35	35.93	35.45	30.40	23.06	18.54	13.83	12.99	4.27	0.43
-0.7	40.32	40.29	40.01	39.10	33.53	27.00	21.61	14.88	14.65	4.85	0.52
-0.6	44.62	44.58	44.23	43.06	37.87	28.54	21.62	18.05	13.93	5.20	0.52
-0.5	49.27	49.16	48.59	47.44	41.31	32.20	25.50	18.19	18.20	5.98	0.66
-0.4	54.06	53.99	53.45	52.09	45.30	36.92	28.78	21.57	20.24	6.57	0.72
-0.3	*58.83	*58.72	*58.18	*56.51	48.63	38.28	30.09	26.11	24.96	7.40	0.96
-0.2	*62.99	*62.86	*61.83	*60.46	50.97	41.62	34.33	28.14	21.65	8.48	1.01
-0.1	*66.06	*65.95	*64.93	*63.26	54.74	44.46	35.64	29.13	26.11	9.73	1.05
0.0	*67.58	*67.42	*66.47	*64.99	54.69	44.12	34.81	31.55	29.22	10.19	1.16
0.1	*67.82	*67.57	*66.42	*63.65	*57.14	46.08	38.61	32.55	29.27	12.03	1.46
0.2	*66.33	*66.02	*64.66	*62.65	53.31	45.78	36.40	32.58	29.12	12.55	1.01
0.3	*63.60	*63.32	*61.73	*60.57	54.27	44.95	37.97	31.65	29.69	13.60	1.78
0.4	*59.61	*59.36	*58.22	*56.22	51.90	41.84	36.86	32.41	29.91	14.82	1.86
0.5	*55.06	54.89	53.66	52.95	44.93	39.25	33.80	29.08	26.98	15.17	2.07
0.6	50.38	50.32	48.94	48.19	41.80	37.28	31.43	29.45	26.88	15.29	1.72
0.7	45.86	45.85	44.60	44.76	39.90	31.38	28.07	28.34	24.00	15.75	2.96
0.8	41.72	41.72	41.61	40.86	35.17	31.12	27.83	25.04	23.28	15.68	3.33
0.9	37.98	37.98	37.62	36.77	33.65	26.27	25.48	23.50	25.54	16.74	3.20
1.0	34.58	34.61	35.03	34.00	31.15	25.14	20.84	22.91	22.46	15.74	3.80
1.30	26.50	26.55	26.06	25.79	23.36	19.50	18.04	17.06	20.44	13.39	4.22

Figure S5 Same as Figure 4 in the manuscript, using an input window ending 20 seconds after the first P-arrival at the closest station, except instead of all stations, only stations within 50 km of the earthquake epicentre are used.

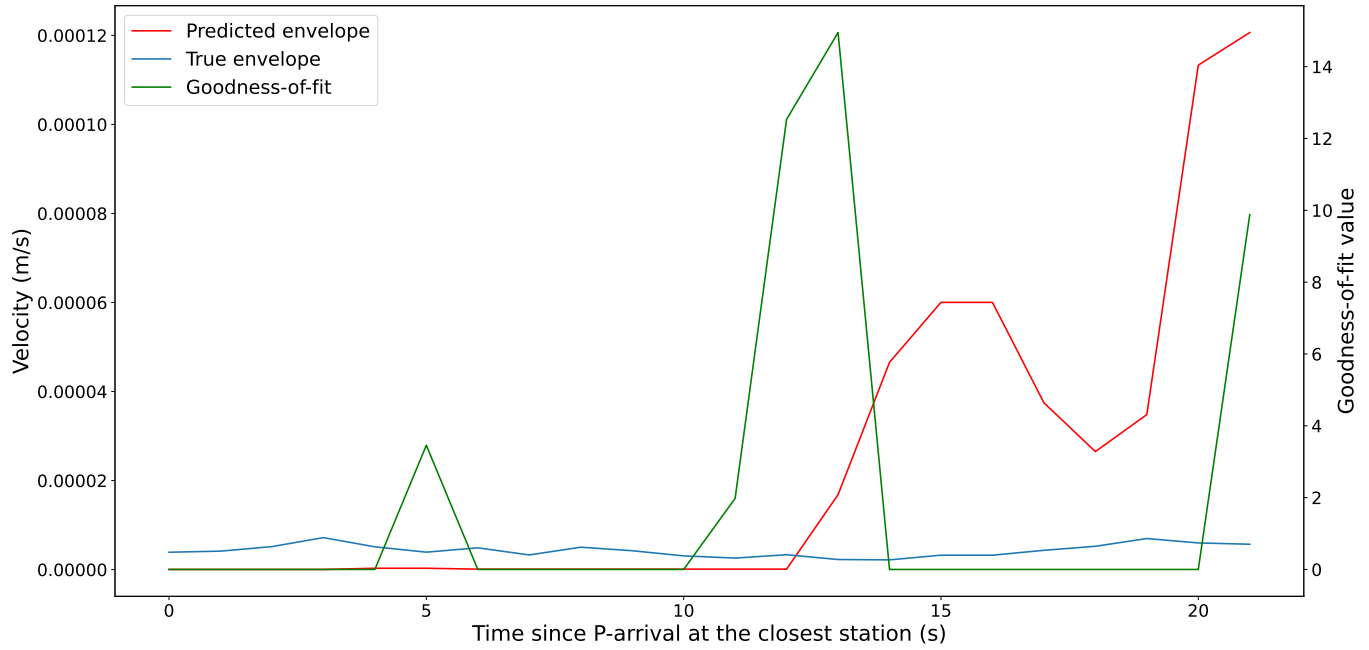

(a) True (blue) and predicted (red) envelopes for station CH.SKRK located 45 km from the wrong epicenter and 83 km from the correct epicenter. Goodness-of-fit evolution over time (calculated using all the envelope data before the specific point in time) is plotted in green. The high background noise at the station means the fit is far from zero. At time t=20 s, the amplitude fit A=12 and the correlation coefficient C=8 give a goodness-of-fit value of G=10.

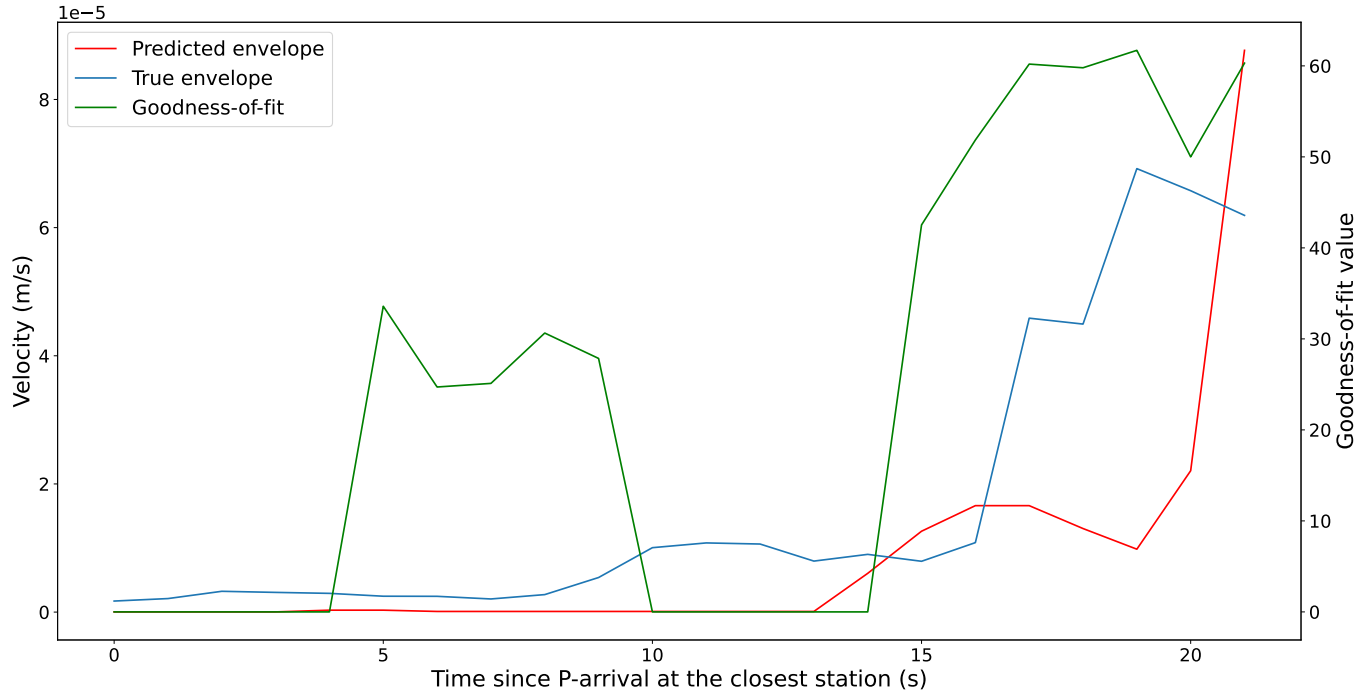

(b) True (blue) and predicted (red) envelopes for station CH.SAPK with a similar distance to the true (52 km) and wrong (49 km) epicentre. Goodness-of-fit evolution over time (calculated using all the envelope data before the specific point in time) is plotted in green. At time t=20 s, the amplitude fit A=48 and the correlation coefficient C=75 give a goodness-of-fit value of G=61.

Figure S6 Examples of situations where a station can have unexpectedly high goodness of fit value even when there is a significant location error. This is a consequence of the inclusion into the GOF calculation of a) more distant stations for which the predicted amplitudes are often close to the noise level, and b) the stations for which the true and false epicentre can be at a similar distance (Figure S6b), e.g. a station halfway between the true and false epicentre. The examples come from the M 3.6 earthquake of 25/10/2020 for which the epicentral location has been moved 100 km from the true epicentre.

2 Envelope prediction

Envelope prediction is carried out using the Cua (2005) envelope prediction relationship, customised for application in Switzerland. The predicted envelopes for a specific location are calculated using magnitude, hypocentral distance and site class (rock or soil). The relationship then provides P and S wave envelopes as outputs, which start at earthquake origin time and are X seconds long, where X is chosen by the user. To attribute the site class to the stations used in this study, we used the EC8 ground types (Code, 2005) available from the SED stations website (Zurich, 1983). For the stations without EC8 ground-type information, a NaN value was assigned. When used in the algorithm the EC8 ground types are categorised as rock (EC8 ground types A and B) or soil (all other EC8 ground types, and NaN values).

The predicted envelopes were initially calculated using a relationship calibrated using data from southern California (Cua, 2005) which consisted of about 30000 records (vertical and horizontal acceleration, velocity, and displacement) coming from 70 southern California earthquakes ($2 \leq M \leq 7.3$) recorded within 200 km from the earthquake source region. However, for the subset of Swiss earthquakes we used (see Data section of the manuscript), we observed (Figure S7) that these predicted envelopes often do not fit the observed shaking well (visual checks showed systematic overpredicting of the observed shaking), with the average amplitude fit *A(S, t)* between the maxima of the predicted and observed horizontal velocity envelopes being 0.83. However, when visually comparing the shapes of the normalised observed and predicted envelopes, we found that in a large majority of the cases, the envelope shape was predicted well. However, when visually comparing the shapes of the normalised observed and predicted envelopes, we found that in a large majority of the cases, the envelope shape was predicted well. Therefore we decided to scale (more details in the next section) the predicted envelopes using the ground motion model (GMM) developed by Cauzzi et al. (2015) for Switzerland (see also Edwards and Fäh, 2013). This approach reduced the difference in peaks between observed and predicted envelopes (Figure S7), with the average amplitude fit *A(S, t)* improved to 0.91. The scaling is done using the PGV of the full predicted envelope, not just the part of the envelope until the current time *t*.

While this significantly improved the overall envelope maximum fit, we still found that the maxima of the P-waves (especially at the closest stations) were higher in the observed data. To further adapt the predicted envelopes, we adopted a station-specific S-to-P scaling factor (Figure S8) that is applied when the predicted envelopes are loaded (calculation of the scaling factors is explained below in the following sections). This led to a slight improvement in the envelope fit. If no S-to-P ratio is available for a station, then the envelope is not corrected and is used as it is.

While the S-to-P scaling factor led to a slight improvement in the results of the method, the rise of the predicted envelopes in the first few seconds after P-arrival at the closest stations was observed to be significantly slower than in the recorded envelopes. To further tackle this problem we multiply the P-wave amplitudes of the closest envelopes (with the P-arrival up to 3 seconds after the P-arrival at the nearest station) by an ad-hoc factor r=3.

2.1 Ground motion model scaling

We use the Swiss ground motion model of Cauzzi et al. (2015) to scale the predicted envelopes and adapt them to Switzerland. The GMM provides estimates on rock-like ground type in the Swiss Alps and Northern Foreland. We used

local site amplification information available for each station in Switzerland (Edwards et al., 2013) to apply station-specific amplitude scaling factors. The GMM uses the moment magnitude Mw which was obtained by converting the local magnitude ML using equation 7 from Edwards et al. (2015). We calculate only the mean horizontal component (the GMM is only defined for the horizontal component) velocity envelopes (we found that the velocity envelopes produce the best fit) and PGV GMM templates. We made sure that we only scale the earthquake envelope, i.e. that the GMM scaling does not affect the noise part of the envelope.

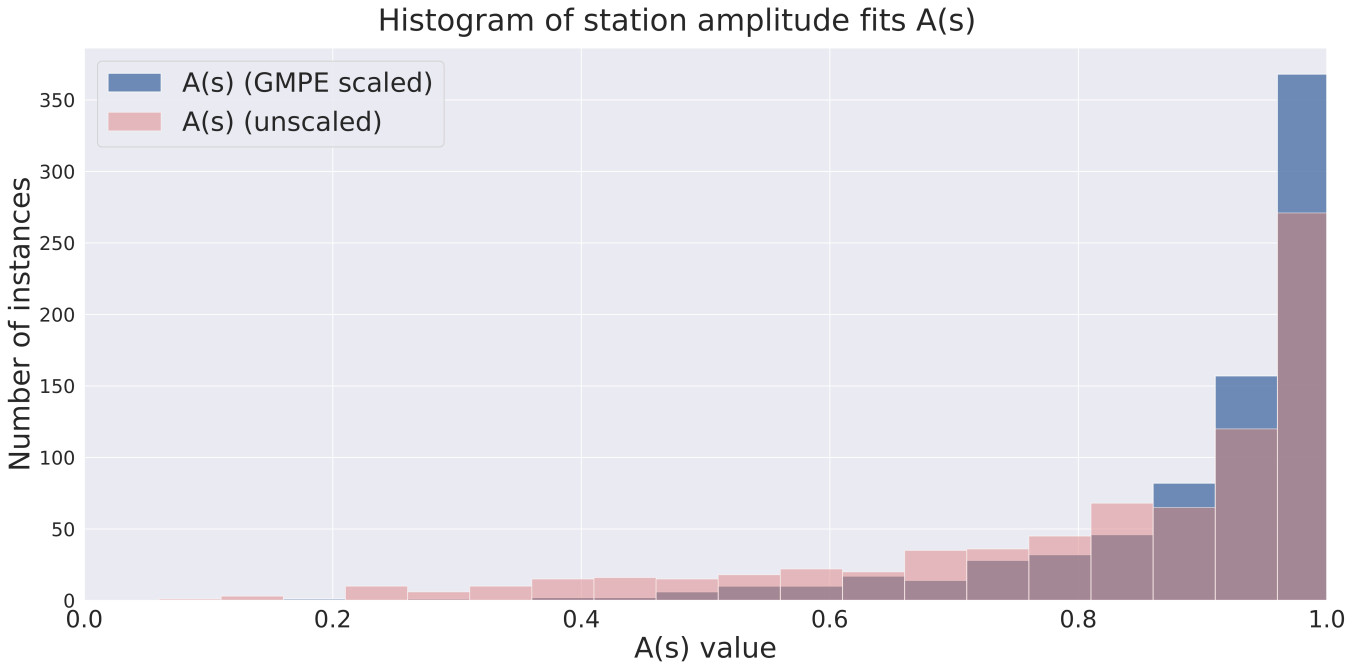

Figure S7 Histogram of amplitude fits A(S, t) between the entire (i.e. with the end time 100 s after origin time) true and predicted envelopes for the Swiss earthquake dataset used in this study (776 envelopes from 10 events). Orange bars represent the fits of predicted envelopes calculated using the Cua (2005) relationship, while the blue bars represent the fits of the envelopes calculated using the GMM-scaled Cua (2005) relationship.

2.2 S-P ratio

We opted for the use of station-specific S-to-P ratios as it is expected to somewhat account for site effects, and also approximately for the path attenuation effects since most of the attenuation occurs in the shallow crust near the receiver (Hardebeck and Shearer, 2003). The station-specific S-to-P ratios used for scaling the envelopes are calculated by using the SeisBench ETHZ dataset (Woollam et al., 2022). We select the horizontal components of the waveforms with associated P- and S-wave arrivals in the dataset metadata. Furthermore, we select only the waveforms from earthquakes with magnitude M>2 (as a proxy for having high SNRs). We combine the two horizontal components into one horizontal component (using root-mean-square). We then calculate the S-to-P ratio for each waveform and exclude those with S-to-P ratios of 20 or higher (we found that the higher ratios were often a consequence of spikes in the data). This reduced the waveform number in the dataset from 36473 to 8300. Finally, we calculate the mean ratio for each station and save it for use during processing.

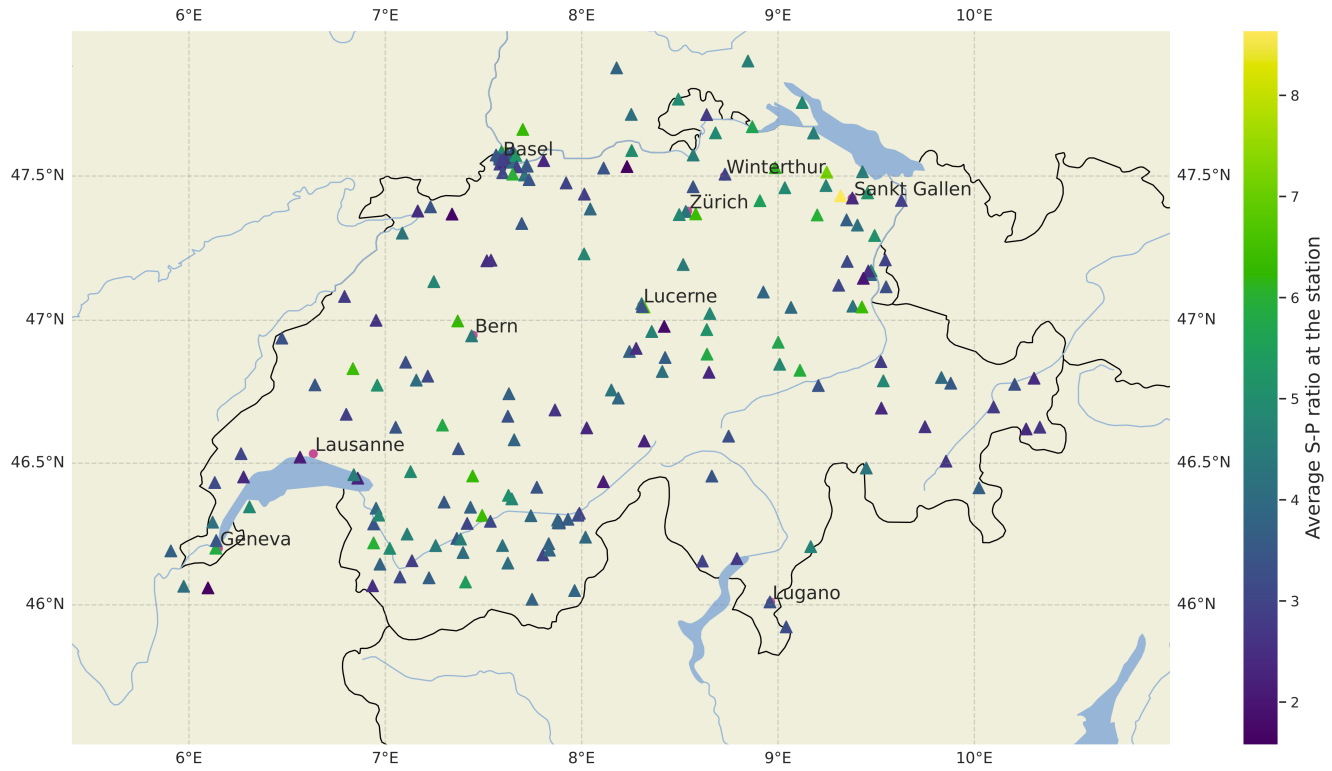

Figure S8 Average S-to-P ratio per station in the CH network.

References

Cauzzi, C., Edwards, B., Fäh, D., Clinton, J., Wiemer, S., Kästli, P., Cua, G., and Giardini, D. New predictive equations and site amplification estimates for the next-generation Swiss ShakeMaps. *Geophysical Journal International*, 200(1):421–438, 2015. doi: 10.1093/gji/ggu404.

Code, P. Eurocode 8: Design of structures for earthquake resistance-part 1: general rules, seismic actions and rules for buildings. *Brussels: European Committee for Standardization*, 2005.

Cua, G. *Creating the Virtual Seismologist: developments in ground motion characterization and seismic early warning*. California Institute of Technology, 2005.

Edwards, B. and Fäh, D. A Stochastic Ground-Motion Model for Switzerland. *Bulletin of the Seismological Society of America*, 103(1):78–98,, 2013. doi: 10.1785/0120110331.

Edwards, B., Michel, C., Poggi, V., and Fäh, D. Determination of Site Amplification from Regional Seismicity: Application to the Swiss National Seismic Networks. *Seismological Research Letters*, 84(4):611–621, 2013. doi: 10.1785/0220120176.

Edwards, B., Kraft, T., Cauzzi, C., Kästli, P., and Wiemer, S. Seismic monitoring and analysis of deep geothermal projects in St Gallen and Basel, Switzerland. *Geophysical Journal International*, 201(2):1022–1039, 2015. doi: 10.1093/gji/ggv059.

Hardebeck, J. and Shearer, P. Using S/P amplitude ratios to constrain the focal mechanisms of small earthquakes. *Bulletin of the Seismological Society of America*, 93(6):2434–2444, 2003. doi: 10.1785/0120020236.

Woollam, J., Münchmeyer, J., Tilmann, F., Rietbrock, A., Lange, D., Bornstein, T., Diehl, T., Giunchi, C., Haslinger, F., Jozinović, D., and Michelini, A. SeisBench—A toolbox for machine learning in seismology. *Seismological Society of America*, 93(3):1695–1709, 2022. doi: 10.1785/0220210324.

Zurich, S. S. S. A. E. National Seismic Networks of Switzerland. *ETH Zürich. Other/Seismic Network*, 1983. doi: 10.12686/SED/NETWORKS/CH.